nature reviews electrical engineering

https://doi.org/10.1038/s44287-026-00331-5

Review article

Check for updates

Multidimensional optical singularities and their applications

Soon Wei Daniel Lim[1,2,3,4], Christina M. Spaegele[1,4] & Federico Capasso[1] ✉

Abstract

Optical singularities are positions in an electromagnetic field in which a parameter such as phase or polarization becomes undefined. These singularities confine light tightly and surround it with steep field gradients, properties now exploited in super-resolution microscopy, sensing and communication. The features themselves have been catalogued for decades under an expanding and partially inconsistent nomenclature. This proliferation of names obscures how few field parameters can be singular and can make it hard to design a singularity. This Review presents an application-driven and mathematically accessible framework in which any singular field reduces to a finite set of fundamental, generic singularities. The robustness of these singularities against small perturbations follows from a topology set by the dimensions of the spaces in which they are defined. We examine forward and inverse methods for designing both stable and unstable singularities, survey their uses across disciplines and consider how higher-dimensional singularities might be reached.

Sections

[1]Harvard John A. Paulson School of Engineering and Applied Sciences, Harvard University, Cambridge, MA, USA. [2]Department of Molecular and Cellular Physiology, Stanford University, Stanford, CA, USA. [3]School of Mechanical and Aerospace Engineering, Nanyang Technological University, Singapore, Singapore. [4]These authors contributed equally: Soon Wei Daniel Lim, Christina M. Spaegele. ✉e-mail: capasso@seas.harvard.edu

Key points

- Singular optics has accumulated a large and inconsistently named catalogue of features, which conceals how few field parameters can actually become undefined and makes these structures harder to design than to observe.

- Every optical singularity can be described through two spaces: one specifying where it is located and one specifying the conditions that must vanish there. The relationship between the dimensions of these spaces determines what shape a singularity takes.

- The same relationship determines whether a singularity survives in the real world. A structurally stable singularity is displaced by perturbations rather than destroyed, provided it carries a topological charge of ±1. Stability also requires that the perturbation fall within its condition space and stay below a limiting magnitude.

- Singularities can be built deliberately, by composing well-understood optical elements or by casting the device as an optimization problem; metasurfaces make it possible to realize both approaches on a single surface. Applications depend on the field surrounding the singularity as much as on the zero itself.

- Because ordinary space offers only three dimensions, the singularities that remain out of reach require synthetic dimensions such as wavelength. Measuring them will in turn require polarimetric sensors able to resolve the fields surrounding a singularity.

Introduction

Optical singularities are positions in an optical field at which one of its parameters, such as the phase or the polarization state, becomes undefined. For example, the wavy bright lines on the bottom of sunlit swimming pools are large-scale singularities of ray optics, known as caustics, where many rays converge[1,2]. In this Review, we focus on singularities in wave optics, which occur at far smaller scales. The canonical example is the phase singularity, a point of undefined phase in a complex scalar field, which appears in random speckle patterns and underpins many imaging and sensing methods. Stefan Hell's Nobel Prize-winning work on stimulated emission depletion (STED) super-resolution microscopy, for example, uses the geometry of a phase singularity to surpass the diffraction limit[3,4]. Such points were first identified as objects worthy of study by Nye and Berry[5], by analogy with dislocations in crystals.

Singular optics extends far beyond phase, and its literature can seem forbidding. It records dozens of named features, from C-loci and V-loci to knots, Möbius strips and skyrmions[6–24], under terminology that is not always consistent[9]. This proliferation obscures a simpler underlying picture. Only a small set of parameters can be singular – phase, field directions, field correlation parameters, spin, polarization-ellipse parameters and the polarization state. Elaborate structures arise by composing these few fundamental singularities or by viewing them in a different space.

Realizing these singularities, however, has long relied on combinations of established wavefront-shaping optics – spatial light modulators, waveplates, holographic elements and related components – each controlling some subset of phase, polarization or spectrum. Metasurfaces, which comprise subwavelength-spaced nanostructures arrayed on a plane[25–28], offer a new approach to compress this range of components onto a single surface with simultaneous control over phase, wavevector, polarization and spectrum[29–33]. This control has widened the range of accessible singularities faster than the descriptive framework has kept up, leaving a gap between the topology that makes a singularity robust and the design choices that produce one. Textbooks[2,34,35] and reviews[36–40] treat singular optics thoroughly, but few connect it to modern wavefront engineering.

This Review addresses that gap with an application-driven and mathematically accessible account for physicists and engineers, covering both the common stable singularities and their rarer unstable generalizations, and treating structural stability as a design parameter rather than a given. We first set out a framework that describes any singularity through the two spaces it inhabits, then use those spaces to explain which singularities survive perturbation and how their topological charge is computed. We next examine the forward and inverse design methods that generate them on metasurfaces and other wavefront-shaping devices, including synthetic dimensions that reach singularities impossible in ordinary space. We then survey the applications their structure enables, from communication and microscopy to precision metrology, linking topology to device function, before closing on where the field may go next.

A framework for optical singularities

To build this framework, we first separate optical singularities from a concept they are commonly conflated with, orbital angular momentum (OAM). The helical phasefront of a cylindrically symmetric OAM beam is often treated as synonymous with OAM, and its on-axis linear phase singularity makes it tempting to equate OAM with optical singularities. However, an optical vortex or OAM-carrying beam is not automatically a singularity. OAM is a property of any beam with a wavefront tilt with respect to the optical axis and does not require a phase singularity. Courtial et al.[41] observed that an elliptical Gaussian beam without a phase singularity can have arbitrary OAM values per photon, as high as $10,000\hbar$. Berry[42] also constructed a beam with axial singularities and a non-zero total topological charge but zero total OAM. Throughout, we reserve 'singularity' for points at which the relevant field parameter is strictly undefined.

We distinguish generic[37] from non-generic singularities. Generic singularities are stable: a small perturbation of the field displaces but does not destroy them, so they persist in the physical world and arise naturally in a wavefield without special symmetry[2,34]. Formally, perturbing the wavefront or wave-generation conditions deforms the singular structure into one related to the original structure by a smooth diffeomorphism[43]. Conversely, non-generic singularities either vanish or split into multiple generic singularities under arbitrarily small perturbations[44]. These perturbations arise from stray light or device imperfections and, to a good approximation, appear as additions or subtractions of plane waves in the neighbourhood of the singularity. For example, phase singularity points in three-dimensional (3D) space[45] are unstable and vanish in the presence of stray light.

Non-generic singularities require a precise coincidence of conditions that are almost never realized spontaneously in random fields or in noisy experiments. They cannot be experimentally generated in a strict mathematical sense, because the slightest experimental imperfection will remove this coincidence. However, if the resulting deviation from the ideal condition overlap is smaller than what the application can resolve, the singularity is effectively realized. Both types of singularities have experimental relevance. Generic singularities are particularly useful in strongly scattering environments, where stability against perturbations, or a perfect zero, is required, as in the coronagraph and phase-retrieval applications described in the 'Imaging and sensing' section in Applications of engineered singularities. Non-generic singularities are suitable in low-scattering, tightly controlled settings or where slight deviation from a perfect zero is tolerable, as in some communication applications ('OAM and communication' section in Applications of engineered singularities). Metasurfaces have produced both generic singularities and approximations of non-generic ones[29–33,46–50].

Structural stability also depends on the medium. The singular structures here are defined in linear media, in which the refractive index is intensity independent. Nonlinear media can support stable singular structures, such as dark vortex solitons in a self-defocusing nonlinear medium. These are localized intensity minima that maintain their shape over time against a bright uniform background, in a medium with negative third-order nonlinear susceptibility[51]. Desyatnikov, Kivshar and Torner review this field in depth[51,52].

Configuration and condition space

Having separated singularities from OAM, we now build the mathematical framework that describes them. To fully design and exploit the topological nature of optical singularities, we must understand their mathematical properties, geometrical structure and structural stability. All singularities can be described by their configuration space and condition space. The configuration space, also known as the control space in wave catastrophe theory[1] and a term from condensed-matter physics[37], specifies the location of the singularity. For the canonical phase singularity in the transverse plane, the configuration space is the two-dimensional space of (x, y) coordinates. Singularities can also be defined in the angular dimension or in synthetic dimensions such as the incident wavelength λ and illumination tilt[33,53] or in frequency-wavenumber space $(\omega, \mathbf{k})$ for spatiotemporal beams[54]. The configuration dimension D_{config}, or domain dimension, is the smallest number of unit vectors needed to specify a position in the configuration space: 2 for the transverse (x, y) plane and 3 for the full Cartesian (x, y, z) space.

The condition space describes what is happening at each position in configuration space and determines whether a singularity exists. Singularities are higher-dimensional zeros of the condition space, located at its origin. For a phase singularity, $\mathrm{Re}(E) = 0$ and $\mathrm{Im}(E) = 0$, so the condition space is $\{\mathrm{Re}(E), \mathrm{Im}(E)\}$, and the singularity exists at its $(0, 0)$ origin.

The condition dimension $D_{\text{condition}}$, sometimes called the co-dimension, is the number of independent homogeneous conditions (equations) specifying the singularity[37]. Equivalently, it is the number of independent constraints on the electromagnetic field[55]. These conditions are homogeneous; they depend on the relative values or the vanishing of parameters, not on their absolute magnitudes. Although D_{config} is chosen by the designer, each singularity class has a fixed condition space (Supplementary Table 1). For example, phase singularities have a fixed co-dimension of two.

Not all field parameters can serve as topologically nontrivial variables: a necessary condition is that the parameter takes negative, zero and positive values, enabling winding behaviour around the zero of the condition space (discussed in Stability and topological charge). An intensity-phase condition space is therefore topologically trivial, because the field intensity is never negative. A more precise formulation of optical fields as maps between configuration and condition space is given in the Supplementary Information.

The generic dimension of a singularity determines the shape it takes in a random wavefield (that is, whether it is a zero-dimensional point, one-dimensional line, two-dimensional surface and so on) and is given by equation (1)

$$D_{\text{singularity}} = D_{\text{config}} - D_{\text{condition}}. \tag{1}$$

This is analogous to the dimension of the solution space in linear algebra, in which the number of unknowns minus the number of constraining equations gives the solution dimension. For example, three unknowns and two constraint equations leave a solution set along a $3 - 2 = 1$-dimensional line.

For a phase singularity in the transverse plane, $D_{\text{config}} = D_{\text{condition}} = 2$, giving $D_{\text{singularity}} = 0$: phase singularities in the complex plane are zero-dimensional points. In the 3D space they become $3 - 2 = 1$-dimensional lines. Singularities have no intrinsic shape; their dimension depends on the configuration space in which they are defined. Similarly, L-loci can be L-points[8], L-lines[6–8] or L-surfaces[12], depending on their embedding configuration space[37]. Supplementary Table 1 lists each singularity type, its existence conditions and its co-dimension. Rather than adopting dimension-presupposing names from the literature (such as C-lines and V-points), we classify by defining conditions and singular parameters, keeping the earliest definitions of the singular parameters but explicitly distinguishing paraxial (transverse) from non-paraxial (full vectorial) cases.

Figure 1 plots representative geometries of common singularity types. Singularities occur at the intersection of the zero-isolines or zero-isosurfaces of individual conditions.

Phase singularities (Fig. 1a) occur when the real and imaginary parts of a scalar field simultaneously vanish, producing positions of undefined phase. The condition values for phase singularities are thus $\{\mathrm{Re}(E), \mathrm{Im}(E)\}$.

The polarization (C, L, V) singularities are most easily described using the polarization ellipse, the closed path that a time-harmonic electric field traces in field space[10]. For the paraxial case, the axes of the space are E_x and E_y, the azimuth is the angle that the major axis makes with the E_x direction, and the handedness is the direction that the electric field traces over time. In the non-paraxial case, the 3D electric field traces an ellipse in (E_x, E_y, E_z) space, and the azimuth becomes a vector along the major axis. The ellipse also has a normal vector, orthogonal to the major and minor axes and oriented so that the ellipse handedness and normal vector obey the right-hand rule.

C singularities (Fig. 1b) occur at points of circular polarization, where no preferred major axis exists and the polarization azimuth is therefore undefined. C singularities have a co-dimension of 2 because two conditions must hold: the major and minor axes must be equal in length, and the field components along these axes must differ in phase by 90°. Paraxial C singularities are zeros of the complex Stokes field $\Sigma = S_1 + iS_2$ (ref. 8), where S_1 and S_2 are the first two Stokes parameters (Supplementary Information). The condition values for paraxial C singularities are thus $\{S_1, S_2\}$.

V singularities are positions of zero vectorial electric field, where the full polarization state is undefined. Paraxial V singularities have $E_{x,y} = 0$, and non-paraxial V singularities have zero longitudinal field as well: $E_{x,y,z} = 0$. Because each time-harmonic field component is a complex number, the condition values for paraxial V singularities are $\{\mathrm{Re}(E_x), \mathrm{Im}(E_x), \mathrm{Re}(E_y), \mathrm{Im}(E_y)\}$ and those of non-paraxial V singularities are $\{\ldots, \mathrm{Re}(E_z), \mathrm{Im}(E_z)\}$.

V-points (Fig. 1c) are a proper subset of paraxial V singularities; they are positions of zero transverse field surrounded by linear or

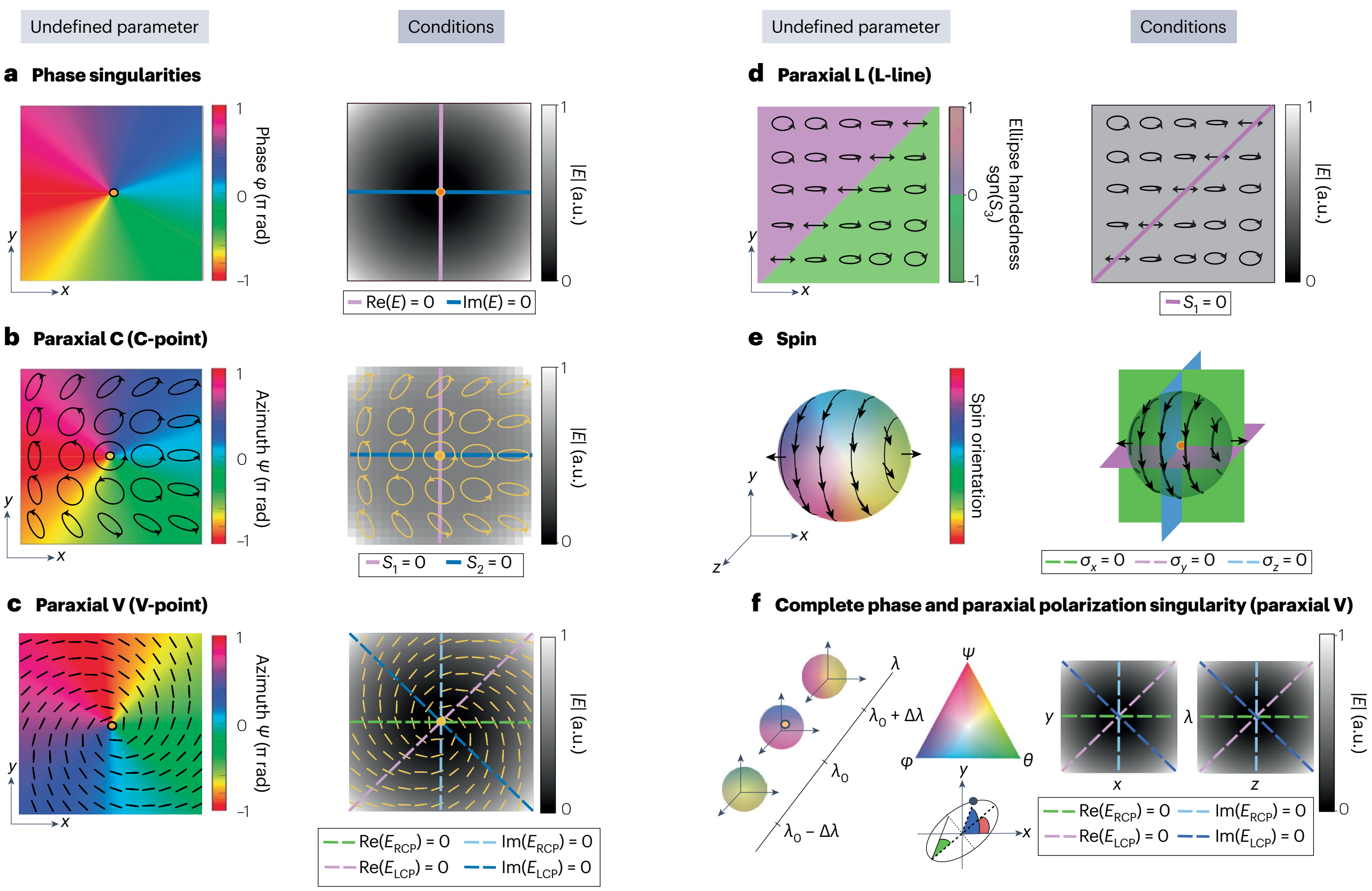

Fig. 1 | Representative geometries of common singularity types. Singularities exist in where all condition values vanish simultaneously, at the origin of condition space. **a**, Phase singularities occur in a scalar field E where the amplitude vanishes, $|E| = 0$. The co-dimension is two, as both real and imaginary parts of E vanish. This produces an intensity zero and generically a vortex-like phase swirl. **b**, Paraxial C-loci (C-points) occur where the polarization azimuth is undefined and the light is circularly polarized; the co-dimension is two, as Stokes components S_1 and S_2 must both vanish. **c**, Paraxial V-loci occur where the transverse field E_x, E_y is zero, giving a co-dimension of four. **d**, Paraxial L-loci occur where the handedness of the polarization ellipse is undefined and the light is linearly polarized. Handedness is the sign of S_3, so the co-dimension is one and these loci form lines. **e**, Spin defect singularities occur where the spin angular momentum density (σ_x, σ_y, σ_z) vanishes[24]. **f**, A complete phase and paraxial polarization singularity resembles a V-point but is defined in four-dimensional space (x, y, z, λ), where it is stable and zerodimensional. Its neighbourhood contains exactly one instance of every polarization state, parametrized by the azimuth Ψ and ellipticity angle θ, including the global phase ϕ. a.u., arbitrary units; LCP, left circular polarization; RCP, right circular polarization.

elliptical polarization[8,14,56] and were originally defined in the transverse plane. However, these singularities are not stable because of the mismatch between the dimensions of the configuration and condition spaces: under perturbation, the V-point splits into multiple stable C-loci[49]. Spaegele et al.[33] created a stable complete phase and paraxial polarization V singularity defined in a four-dimensional (x, y, z, λ) configuration space (Fig. 1f), realizing every transverse polarization state, including the global phase, in its four-dimensional vicinity.

L singularities are positions of linear polarization where the normal of the polarization ellipse is undefined. Paraxial L singularities (Fig. 1d) are commonly known as L-lines in the transverse plane[8,10]. The direction of the ellipse normal (into or out of the plane) follows from the ellipse handedness, which is set by the sign of the z-directed spin angular momentum (SAM), proportional to the real-valued S_3 Stokes parameter. When $S_3 = 0$, the ellipse collapses into a line, so the normal is undefined, producing the singularity. S_3 is the only condition value for this $D_{\mathrm{condition}} = 1$ system, making it generically a line in the transverse plane. Non-paraxial L singularities, however, have a co-dimension of 2 because they involve the normal vector of the 3D polarization ellipse, which has two components[37].

A spin defect singularity with $D_{\mathrm{condition}} = 3$ (Fig. 1e) has also been identified[24]. This is the position where the total SAM density of light, $\boldsymbol{\sigma} = (\frac{1}{4\omega})[\epsilon_0 \mathrm{Im}(\mathbf{E}^* \times \mathbf{E}) + \mu_0 \mathrm{Im}(\mathbf{H}^* \times \mathbf{H})]$ vanishes. Because the SAM density is a vector with three independent components, its condition values are $\{\sigma_x, \sigma_y, \sigma_z\}$.

Coherence singularities, singularities in the degree of correlation of electromagnetic fields, also exist[34], though they are less studied. Singularities in the cross-spectral density[57] and mutual coherence function[58] are singularities in the complex phase of a scalar field and thus have a co-dimension of 2.

These fundamental singularities combine into more elaborate structures, including knots[19,59,60], 3D skyrmions[23,61,62], skyrmionic hopfions[22] and optical Möbius strips[20,21] (half-integer twisting of a polarization major axis around tightly focused polarization singularities), as well as the star, monstar and lemon variants of C-loci. We focus here on the fundamental constituent singularities and leave optical skyrmions to the dedicated review of Shen et al.[63].

Supplementary Table 2 presents each singularity class organized by the dimensions of configuration and condition space. Whether a given singularity can exist stably in the physical world depends on the relationship between these two dimensions — the subject of the next section.

Stability and topological charge

The stability of a singularity is set by the relationship between its two dimensions. A generic singularity of dimension d must satisfy $D_{\mathrm{config}} = D_{\mathrm{condition}} + d$; this is the first design rule. Because there are only three Cartesian spatial dimensions, singularities with a co-dimension larger than 3 cannot exist stably in ordinary space, and reaching them requires additional synthetic dimensions: system parameters such as wavelength or angle of incidence that act as extra configuration coordinates. Satisfying the dimension rule is necessary but not sufficient: a generic singularity must also carry a topological charge of ±1 (ref. 64), an integer that counts how many times the surrounding field wraps around the singularity. This section connects topological charge to the field structure around a singularity and to its stability.

Structural stability is the continued existence of a singularity under a small perturbation ε in the fields or condition values[37]. A structurally stable singularity is shifted within configuration space but does not vanish (Fig. 2a). Such behaviour holds because a generic singularity has all possible condition values, up to normalization, in the immediate vicinity of the zero, so the surrounding condition values can cancel arbitrary but small perturbations. Each value occurs only once; by contrast, higher-order singularities of charge m repeat each condition value m times and split into m generic singularities under perturbation[44].

Singularity stability holds only up to a limit. A perturbation with magnitude larger than the surrounding field values can destroy the singularity. The 'strength' of the stability is the maximum perturbation magnitude for which the singularity enforces destructive interference. This is distinct from the topological charge, sometimes called the dislocation strength[37]. For a phase singularity, this 'strength' is the largest field magnitude range $\sqrt{\mathrm{Re}(E)^2 + \mathrm{Im}(E)^2}$ over which all phases occur, and a perturbation exceeding that range makes the singularity vanish. A wide stable range is therefore desirable.

Singularities are only robust against perturbations in the field properties that span their condition space. A paraxial C-point is stable against small paraxial-polarization perturbations, but a non-paraxial polarization perturbation will destroy it, because the surrounding field does not protect against E_z perturbations.

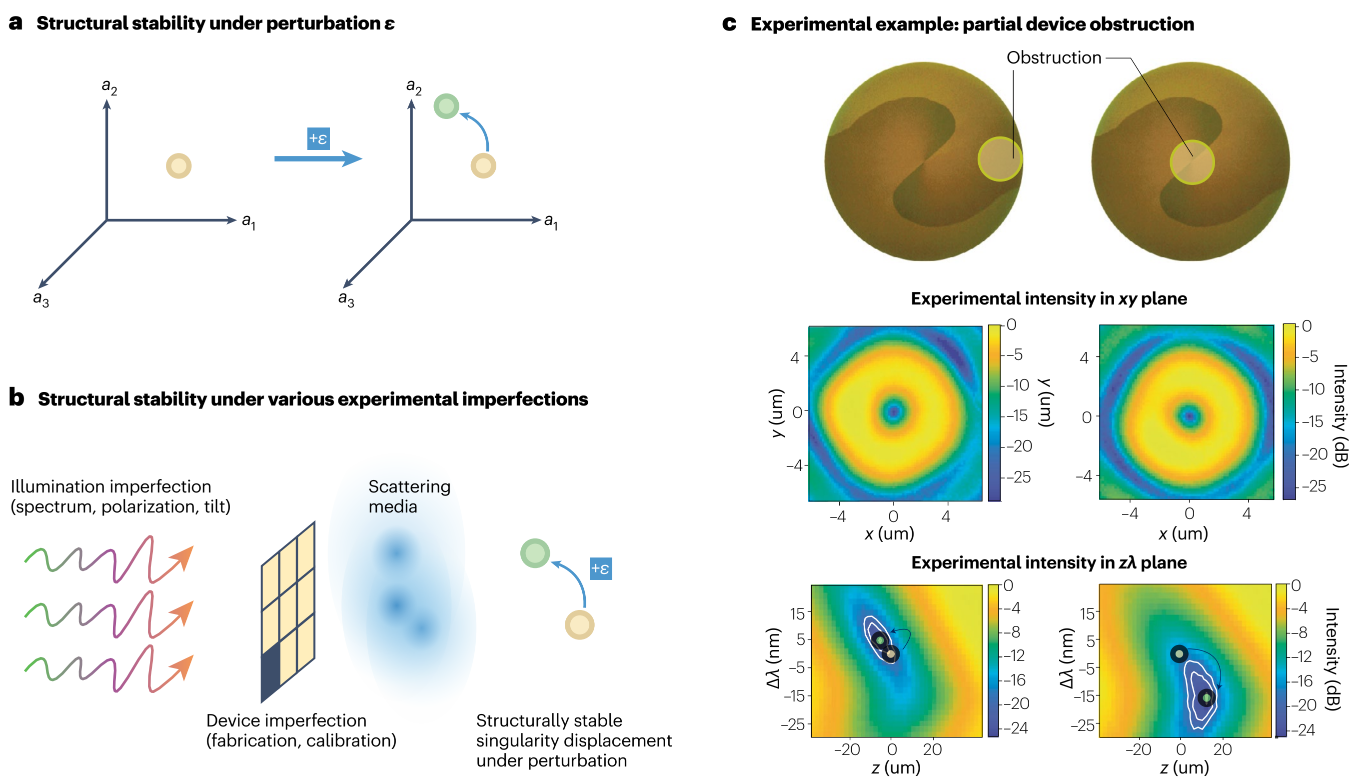

Fig. 2 | Structural stability and singularities. a, Structural stability is the continued existence of a singularity under a small perturbation ε of the conditions $\{a_1, a_2, a_3\}$. ε is an additive shift in the condition values, such as stray light adding to the complex field. Structurally stable singularities are displaced in space by such a perturbation but do not vanish. **b**, Perturbations can arise from imperfections in the illumination state (spectral content, polarization or geometrical tilt), in device design and fabrication or from weakly scattering and absorbing propagation media. **c**, Experimental demonstration of a device imperfection perturbing a structurally stable polarization singularity defined in (x, y, z, λ) configuration space[33]. Part of the metasurface generating the singularity was obstructed by an opaque disk in two locations over two experiments; the singularity persisted and was observed to displace mainly in (z, λ) space from its design position. Panel **c** is adapted with permission from ref. 33, AAAS.

Perturbations can also arise indirectly, from imperfect illumination, device design or propagation media (Fig. 2b), which effectively add or subtract fields at singular positions. Structurally stable singularities shift rather than vanish under such imperfections. This robustness and the role of synthetic dimensions in reaching it are illustrated by the paraxial V singularity: a co-dimension-4 zero that is unstable in the 3D space becomes a stable zero-dimensional point once defined in the four-dimensional (x, y, z, λ) space introduced earlier. Spaegele et al.[33] confirmed this prediction experimentally, obscuring part of the generating metasurface and observing the singularity persist, displacing mainly in (z, λ) space rather than disappearing (Fig. 2c).

Fundamental singularities remain stable in realistic physical media with turbulent refractive-index fluctuations as long as the perturbing field is weaker than their stability strength; composite structures need not. This robustness matters for communication, metrology and sensing[65,66]. Pires et al.[66] showed that superposed phase-singularity lines and rings are stable only under small perturbations and transform into other knot types under stronger ones – the more stable the fundamental singularities, the more stable their composite. Where perturbation sources can instead be suppressed by fabrication precision or stray-light elimination, even topologically unstable singularities can perform adequately for a given application.

Two methods determine whether the topological charge is ±1: the degree of the mapping between configuration and condition space[67,68], and the sign of the Jacobian determinant at the singularity. The charge also appears in the literature as the vortex charge, Hopf index or singularity index. In two dimensions, the degree of a mapping is the winding number, which counts how many times a curve loops around a point, such as the origin of condition space[38], with sign set by the curve orientation (Fig. 3a). For an optical singularity, we encircle it in configuration space with an anticlockwise curve and count the windings of the corresponding trajectory around the condition-space origin (Fig. 3b, middle row).

For phase singularities in two dimensions, the winding number m follows from equation (2), which accumulates the complex phase over an anticlockwise loop C around the singularity

$$m = \frac{1}{2\pi}\oint_C \mathrm{d}\phi = \frac{1}{2\pi}\oint_C \nabla\phi \cdot \mathrm{d}\mathbf{r}, m \in \mathbb{Z}. \tag{2}$$

This integral tracks the winding number of the trajectory in $\{\mathrm{Re}(E), \mathrm{Im}(E)\}$ condition space. m must be an integer, because a closed path returning to the start must accumulate a phase equal to 0 modulo 2π. The winding number is unchanged when the path is continuously translated or distorted in configuration space, and changes only by integer increments when phase singularities move into or out of its interior.

For the canonical transverse phase singularity at (x_0, y_0), the mapped curve wraps once around the origin of condition space

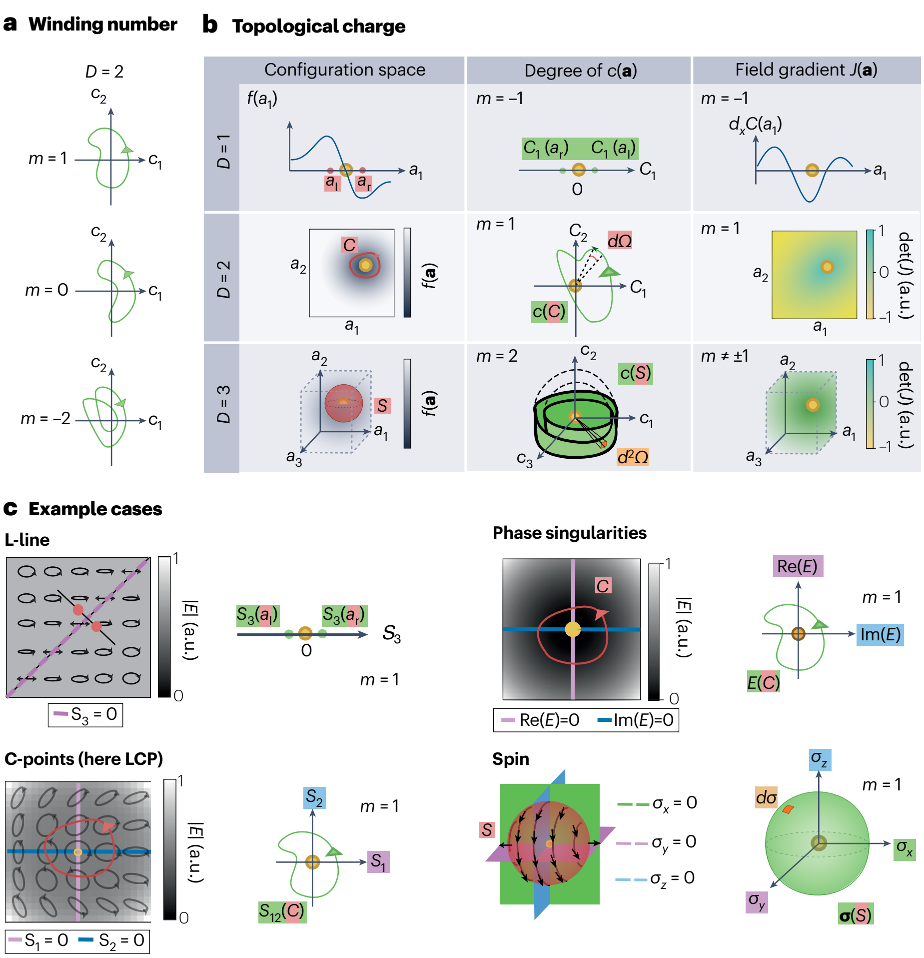

Fig. 3 | Generalized structural stability and topological charge for arbitrary-dimensional singularities. Only zero-dimensional point singularities with $D_{\mathrm{config}} = D_{\mathrm{condition}} = D$ are considered here. **a**, For $D = 2$, encircling a singularity in configuration space maps to a trajectory in $\{c_1, c_2\}$ condition space (green loop) that winds around the origin an integer number of times: the winding number, identifying the topological charge. **b**, In other dimensions the charge follows from the degree of a continuous mapping. Each row shows the singularity in configuration space (first column), the charge computation (second column) and the field gradients, parametrized by the Jacobian determinant (third column). For $D = 1$, the singularity is bounded by two points whose condition values set the charge; for $D = 3$ it is enclosed by a spherical shell, and the number of times the corresponding condition–space shell wraps the origin gives the charge. **c**, Charge calculations for common optical singularities. Paraxial L-loci (L-lines), of co-dimension one, take their charge from the sign jump of S_3 Stokes parameter across the singularity. Phase singularities and paraxial C-loci, of co-dimension two, use the winding number. The spin defect singularity, of co-dimension three, uses the mapping between spherical shells in configuration and spin space.

(Fig. 3c, top right), giving $m = 1$, with all condition values appearing once in the immediate vicinity.

This stability mechanism generalizes to arbitrary dimensions[67]: as long as the map from the immediate vicinity of the singularity attains all possible condition values once (up to normalization), the singularity is structurally stable. For simplicity, we specialize to point (zero-dimensional) singularities, which occur generically only when $D = D_{\mathrm{config}} = D_{\mathrm{condition}}$; this restriction lets us identify correspondences with common concepts in topology.

With a one-dimensional condition space, singularities are the zeros of a one-dimensional function $f(a_1)$ (Fig. 3b, first row). The topological charge is the change in function sign across the zero, or equivalently, the sign of the function slope there. With a two-dimensional condition space $\{c_1, c_2\}$, it is the winding number of the loop C (Fig. 3b, middle row). With a 3D configuration space, we consider a spherical shell S around the singularity and count how many times the condition values on this surface wrap around the origin of the condition space (Fig. 3b, bottom row). Mapping degrees in higher dimensions are difficult to visualize, because they measure how often a $(D_{\mathrm{condition}} - 1)$-dimensional surface wraps around the origin of the $D_{\mathrm{condition}}$-dimensional condition space[67], but equation (3) computes them

$$l = \frac{1}{A}\oint_S \mathrm{d}^{D_{\mathrm{condition}}-1}\Omega, \quad l \in \mathbb{Z}. \tag{3}$$

Here $\mathrm{d}^{D_{\mathrm{condition}}-1}\Omega$ is a differential solid angle in $D_{\mathrm{config}} = D_{\mathrm{condition}}$ dimensions, and A is the total solid angle of a $(D_{\mathrm{condition}} - 1)$-sphere. For $D_{\mathrm{condition}} = 2$, a 1-sphere is a circle, so this reduces to the familiar loop integral with $\mathrm{d}^{2-1}\Omega = \mathrm{d}\phi$ and $A = 2\pi$. In all these calculations of topological invariants, the trajectory C or shell S must not pass through the singularity itself. This ensures that the fields are well-defined at every integration position.

Figure 3c shows the topological charge calculation for four representative singularities. For $D_{\mathrm{condition}} = 1$, paraxial L singularities (Fig. 3c, top left) have a charge equal to the S_3 sign change across the singularity, $2l_L = \mathrm{sgn}[S_3(a_r)] - \mathrm{sgn}[S_3(a_l)]$, in which a_r and a_l bound the L locus on the right and left, respectively. In two dimensions, phase singularities (top right) and paraxial C singularities in the transverse plane (Fig. 3c, bottom left) both use the winding number, computed identically for condition spaces $\{\mathrm{Re}(E), \mathrm{Im}(E)\}$ and $\{S_1, S_2\}$, respectively. For $D_{\mathrm{condition}} = 3$, the spin-defect charge is the degree of the continuous mapping between a thin spherical shell in Cartesian space $\{x, y, z\}$ and the corresponding surface in SAM space $\{\sigma_x, \sigma_y, \sigma_z\}$ (Fig. 3c, bottom right). The Supplementary Information gives the charge of C and V singularities.

The conventional V-point[8,14,56] (transverse field zero $E_{x,y} = 0$ surrounded by linear or elliptical polarization) admits a similar integer, the Poincaré–Hopf index, from accumulating the polarization azimuth on a closed loop. This index is topological, invariant under continuous deformations of the integrating curve that avoid the singularity, yet the V-point is not structurally stable. Any perturbation, including linearly polarized stray light, removes the field zero[49], because the V-point is surrounded by all linear polarization azimuths but not all complex states of linear polarization (their phases). This instability reflects the mismatch between the condition dimension (four) and the configuration dimension (two). A topological charge alone does not guarantee structural stability; only charges of the form of equation (3) with $D_{\mathrm{config}} \geq D_{\mathrm{condition}}$ are stable.

For well-behaved analytic mappings, the charge calculation simplifies to a Taylor expansion near the singularity (Fig. 3c, right column). Let the vector of condition values be $\mathbf{C} \in \mathbb{R}^{D_{\mathrm{condition}}}$ and a configuration-space position be $\mathbf{a} \in \mathbb{R}^{D_{\mathrm{config}}}$. At a singularity $\mathbf{a}_0$, $\mathbf{C}(\mathbf{a}_0) = \mathbf{0}$, and the multivariate Taylor expansion about $\mathbf{a}_0$ is, to leading linear order,

$$\mathbf{C}(\mathbf{a}) = \mathcal{J}\,(\mathbf{a}_0)(\mathbf{a} - \mathbf{a}_0) + O(|\mathbf{a} - \mathbf{a}_0|^2), \tag{4}$$

where $\mathcal{J}$ is a $[D_{\mathrm{condition}} \times D_{\mathrm{config}}]$ real-valued Jacobian matrix of first derivatives: $(J_{ij}) = \frac{\partial C_i}{\partial x_j}$, with C_i the ith condition value and x_j the jth configuration coordinate. The Jacobian matrix is the higher-dimensional analogue of the gradient.

If the Jacobian determinant is non-zero (and $D_{\mathrm{condition}} = D_{\mathrm{config}}$), the singularity carries a charge of $m = \mathrm{sgn}(\det\mathcal{J}) = \pm 1$ and is stable[33,69]. If $\det\mathcal{J} = 0$, the singularity has trivial topology ($m = 0$) or is of a higher order, and is unstable. The approach cannot evaluate non-generic higher-order singularities with $|m| > 1$, which need the earlier high-dimensional integral or a higher-order Taylor expansion.

Designing a generic singularity therefore requires two conditions: its dimension equals $D_{\mathrm{config}} - D_{\mathrm{condition}}$, and its topological charge is ±1.

Designing singularities

Knowing which singularities are stable and how to compute their charge, we turn to realizing them in a device. Two complementary approaches exist: forward design, which composes well-understood building blocks, and inverse design, which casts the device as an optimization over its physical parameters. The two are often combined.

Forward design

Forward design composes well-understood components into a larger device. These components can be physical elements, such as individual nanostructures, or field decompositions where each field component is understood and can be realized directly. Forward design works well when the desired optical field distribution over the domain is known, as for a simple phase singularity with analytical azimuthal dependence $e^{i\theta}$.

The desired field can be decomposed into simpler elements (such as well-understood field profiles[70], plane waves[7,71,72], Bessel beams[70,73] or Laguerre–Gaussian beams[59,74]) that can be individually realized and re-composed. For polarization-dependent fields, each basis weight can be replaced by a Jones matrix[75]. Scalar fields can also be reconstructed using iterative (for example, computer-generated holography) or non-iterative analytic processes[76].

Those basis components can be individually created with optical elements such as spatial light modulators (SLMs)[17,40,77], waveplates[78,79], q-plates[80], holographic plates[81], pinhole interferometers[82,83] and photonic crystals[84]. For example, combining multiple SLMs (or a single SLM with split regions) and waveplates gives dynamic control over amplitude, phase and polarization[85], at the cost of low efficiency and a larger footprint. Metasurfaces improve both by integrating multiple optical functions into a single device, superposing the propagated decomposition components on the metasurface plane and implementing them through unit-cell approaches[75]. They are particularly well suited to spatially varying polarization transformations and structural birefringence[86,87]. Although metasurfaces are still used mainly for passive applications, research into active metasurface control is advancing quickly[88].

Identifying a suitable optical field in the first place is itself difficult. Although some singular structures have an analytic closed form (such as some knots[59] and spin defect singularities[72]), in general, the singular behaviour of a field does not determine its wider behaviour away from the singularity. Many fields can therefore realize the same singular behaviour, although these fields are not equally useful or accessible. The optimal field distribution for a given set of singular characteristics is often difficult to know a priori. Even when the field distribution is known, selecting the appropriate modes and their weights can be challenging[38]. In such cases, and when the design parameters relate to the resultant fields in non-obvious ways, inverse design becomes useful.

Inverse design

Inverse design expresses the device as an optimization problem over its realizable parameters (such as pixel states on an SLM or meta-element shapes on a metasurface), achieving the desired fields by maximizing or minimizing one or more objective functions[89,90]. It is ideal for nanofabricated metasurfaces and photonic crystals, given their large design space. We consider two recent uses: engineering structurally stable generic singularities and non-generic singularities.

For generic singularities, inverse design improves upon any step of forward design. For example, after a set of basis waves is selected, inverse design refines their decomposition coefficients to maximize structural stability against fabrication imperfections and misalignment, using the field intensity as the objective function[59]. For high-dimensional singularities, $\det\bar{J}$ can serve as the objective function, because maximizing its magnitude minimizes singularity displacement under perturbation. Inverse-designing the Jacobian itself, for example, through its singular value decomposition, gives further control over the orientation and skew of the singularity[33].

When the mathematical decomposition is known, inverse design maps the nanophotonic device geometry to the desired transmission function. This is called topology optimization, a variant of which Wang and Fan implemented to fine-tune arbitrarily tilted spatiotemporal optical vortices through constrained optimization[72].

The hardest aspects of inverse design remain choosing an appropriate objective function and a good starting point; forward design can identify a promising initial guess, increasing the likelihood of reaching good solutions.

Although non-generic singularities do not physically exist in a strict mathematical sense, their idealized form can be approximated through precise alignment of wavefront-shaping components, elimination of stray light, or restriction to configurations preserving the requisite system symmetry. For example, $l = 2$ vortices were used in optical vortex grating coronagraphs for their better filtering performance than $l = 1$ and $l = 3$ vortices when imaging near bright stars[91], an application that preserves the circular symmetry of the higher-order vortex configuration.

Non-generic singularities with shape dimensions that differ from $D_{\mathrm{config}} - D_{\mathrm{condition}}$ can also be inverse-designed. Points satisfying each singularity condition individually are $(D_{\mathrm{config}} - 1)$dimensional sets: lines in a two-dimensional configuration space (Fig. 1a–d, zero-condition isolines), surfaces in a 3D configuration space (Fig. 1e) and so on. The singularity exists at their intersection. The gradient vector of a scalar field points in the direction of maximum increase and is thus orthogonal (in a Euclidean sense) to the level set through that point (Fig. 4a).

Surfaces intersect generically along a line, with gradient vectors pointing in different directions but can also intersect degenerately (Fig. 4a–c). The intersection locus can be aligned (Fig. 4b), when the curvature orientations of the level sets match, or anti-aligned (Fig. 4c), when they are opposite, independently of the gradient direction. The aligned case lets the singularity extend in the tangent plane of the intersection, whereas the anti-aligned case does not; the aligned case is therefore useful for engineering a region of extended overlap, such as a sheet singularity[31] (Fig. 4d). The anti-aligned case is useful in engineering an isolated dark point surrounded by light[32]. When the two surfaces coincide, their intersection is a two-dimensional membrane sheet singularity[31]. These degenerate intersections are fragile: slight misalignment makes the surfaces intersect generically or not at all.

The condition surfaces can be aligned by treating the design as an optimization and maximizing the alignment of the level set shapes at the desired singularity position. Lim et al.[31,32] proposed the

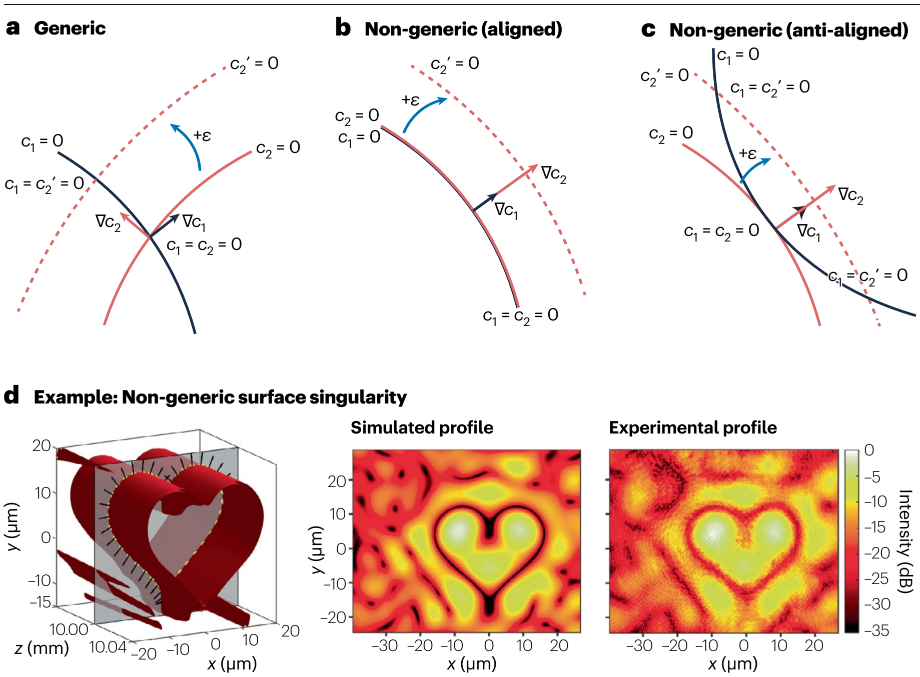

Fig. 4 | Generic and non-generic intersections, depicted using condition-value isolines on a two-dimensional plane. Two condition isolines intersecting generically do so at a point, their gradient vectors pointing in different directions. **a**, Gradient vectors point in the direction of maximum increase and are normal to the isoline. **b**,**c**, When the gradient vectors of two isolines point in the same direction at the intersection, the isolines can be aligned (**b**) or anti-aligned (**c**). Aligned isolines approximate an intersection along an extended locus, producing a higher-dimensional singularity. Anti-aligned isolines can produce point phase singularities in three-dimensional space if the zero level sets separate away from the two-dimensional plane. **d**, A non-generic aligned surface singularity with a heart-shaped cross-section, obtained by aligning the condition gradient vectors (black arrows) along a heart-shaped contour (yellow dots). Numerically simulated (middle) and experimentally measured (right) intensity profiles in the plane $z = 0$. Part **d** is adapted from ref. 31, CC BY 4.0.

phase-gradient magnitude as one component of the objective function, showing that point and sheet singularities form when it is maximized along specified directions. The phase gradient $\nabla\phi$ is the spatial gradient of the field complex phase ϕ. A complex scalar field in polar form, $E(\mathbf{r}) = A(\mathbf{r})\exp[i\phi(\mathbf{r})]$, expresses the phase gradient through the gradients of its real and imaginary components $\nabla\mathrm{Re}(E)$, $\nabla\mathrm{Im}(E)$ (equation (5))

$$\nabla\phi = \mathrm{Im}\left(\frac{\nabla E}{E}\right) = \frac{\mathrm{Re}(E)}{\mathrm{Re}(E)^2 + \mathrm{Im}(E)^2}\nabla\mathrm{Im}(E) - \frac{\mathrm{Im}(E)}{\mathrm{Re}(E)^2 + \mathrm{Im}(E)^2}\nabla\mathrm{Re}(E). \quad (5)$$

Maximizing $\nabla\phi \cdot \hat{n}$ along a direction $\hat{n}$ simultaneously maximizes the field gradients $\nabla\mathrm{Re}(E)$, $\nabla\mathrm{Im}(E)$ across the singularity position and minimizes the field magnitude $|E|^2 = \mathrm{Re}(E)^2 + \mathrm{Im}(E)^2$. The latter enforces singular behaviour (that is, moving the zero level sets to that position), whereas the former improves the spatial confinement of the singularity along $\hat{n}$. Tighter spatial confinement is useful for optical trapping.

This method extends to other singularity configurations by replacing the field gradients $\nabla\mathrm{Re}(E)$, $\nabla\mathrm{Im}(E)$ with condition-value gradients $\{\nabla c_i\}$, and the field intensity $|E|^2$ with a (possibly weighted) sum over condition magnitudes $\sum_i |c_i|^2$.

Applications of engineered singularities

Engineered singularities, and the singular light fields around them, underpin a broad range of applications (Box 1). Because each application exploits the field in the immediate neighbourhood of a singularity, these are more accurately described as applications of singular light fields rather than of the singularities themselves.

OAM and communication

Using OAM-carrying modes for classical communication[92–95] and quantum communication[96–101] exploits modal orthogonality, which in turn requires phase singularities. Information can be multiplexed onto a set of spatially overlapping scalar modes and later demultiplexed only if these modes are mutually orthogonal, that is, their inner product vanishes. For modes that occupy the same transverse region, this orthogonality forces all but one of the modes to have field zero-crossings. These nodal lines or surfaces are themselves phase singularities (Supplementary Information).

These nodal singularities have not been explicitly engineered for communication, raising the possibility of deterministically positioning them at known obstacle locations to communicate around the obstacles with minimal scattering loss. In Hermite–Gaussian and Laguerre–Gaussian modes, nodal positions form straight lines and concentric circles in the transverse plane, corresponding to nodal sheets and cylinders in the 3D space.

In classical communication, OAM modes raise the information transmission rate by increasing the number of orthogonal channels in spatial mode-division multiplexing. For quantum communication, this advantage goes beyond transmission rates. Quantum key distribution is a provably secure method for two parties to share a secret key while detecting unauthorized interception. Quantum protocols typically transmit quantum bits, or qubits, which are two-state systems such as the direction of photon polarization. Increasing the number of levels, as with OAM states, produces qudits with $d > 2$ levels, yielding higher information flux and improved security, because eavesdroppers can be detected more easily[102,103]. Quantum key distribution with multiple OAM states has been demonstrated in free space[98], underwater[100] and through air-core fibre[101]. Beyond scalar spatial modes, vectorial modes with spatially varying polarization further expand the parameter space. Quantum communication with fully non-paraxial modes, using all three Cartesian field directions, has also been demonstrated[104], opening the way to still higher-dimensional modes.

Imaging and sensing

Berry conjectured that structurally stable, generic singularities could serve as a 'skeleton' for the wavefield, around which the global wave behaviour can be constructed[43]. Because phase singularities are generic, they serve as robust markers for tracking the evolution of a field[105,106]. The positions of intensity zeros on a two-dimensional transverse plane also improve the starting guess for phase-retrieval algorithms in image reconstruction[107,108].

Singularities also reflect the coherence and tilt properties of the illuminating field. A vortex plate produces a true intensity zero only for coherent, normally incident light, because incoherent and off-axis light cannot interfere destructively to zero. Swartzlander proposed a vortex-beam phase mask that suppresses coherent, on-axis

Box 1 | Applications of optical singularities

Communication

Modes with different topological charges can multiplex and demultiplex information in optical communication systems, increasing bandwidth for classical communication or improving the security of quantum communication.

Imaging and sensing

Vortex coronagraphy: optical singularities act as spatial filters that suppress unwanted detection regions, suppressing on-axis light to reveal off-axis sources.

Precision localization metrology

The tight localization and steep gradients surrounding optical singularities suit them to precision localization metrology, as optical rulers or as structured beams in super-resolution microscopy techniques such as STED and MINFLUX. MINFLUX improves the spatial resolution of fluorescent STED microscopy by localizing molecules at the zero-intensity points of a pump beam.

Micromanipulation

The tight localization of dark singularities and the ability to design their polarization-dependent environment suit them to trapping and manipulating particles and to high-precision photon-based micromachining.

Superoscillation profiling and control

Optical singularities enable superoscillations, which have been used to generate focal spots smaller than the diffraction limit or highly directed signals.

Modelling phenomena

Optical singularities model complex phenomena across physics by serving as scalable, controllable laboratory-scale proxies, giving access to high-dimensional geometries and topological states.

illumination relative to incoherent or off-axis sources[109]. This underlies the optical vortex coronagraph[91], which suppresses the bright on-axis star in astronomical imaging so that peripheral objects can be detected. Charge-2 vortices give better contrast than charge-1 or charge-3 (ref. 91), and only the charge-2 mask has the correct geometrical symmetry for quasi-achromatic subwavelength-grating coronagraphs[110]. An annular-groove vortex coronagraph on the 10 m Keck II telescope resolved a brown dwarf 186.5 milliarcseconds from its host star[111].

Precision localization metrology

The steep, tightly localized phase gradients around a singularity are narrow, high-spatial-frequency features that track minute displacements. Yuan and Zheludev[112] used this property to create an optical ruler with subnanometre resolution, resolving displacements of $\lambda/800$ by tracking high-phase-gradient features, compared with $\lambda/3$ resolution when tracking bright peaks.

Liu et al.[113] later applied machine learning to scattered light fields, reconstructing nanowire displacements to better than 92 pm (or about $\lambda/5,300$), as large momentum transfers in high-phase-gradient regions make the scattered field strongly dependent on nanowire position.

Even without phase resolution, field zeros can be localized more precisely than field maxima because of shot noise. Treating photons with Poisson statistics, the expected number of events $E[N]$ is proportional to the light intensity, and the standard deviation in N is $\sqrt{E[N]}$. Xiao and Ha provide a simple model connecting shot noise to localization precision, treating two positions as resolvable if their intensity difference exceeds the standard deviation[114] (Supplementary Fig. 1). For an intensity maximum with expectation $N_{\max} \gg 1$, the large standard deviation $\sqrt{N_{\max}}$ means a broad range of points have signal intensities consistent with the true maximum, yielding poor localization (Supplementary Fig. 1a). For an intensity minimum with the same local intensity curvature, the smaller $N_{\min}$ yields a smaller $\sqrt{N_{\min}}$ and tighter localization (Supplementary Fig. 1b). If the intensity minimum is a phase singularity, $N_{\min}$ approaches zero, bounded only by background. Wolter used this effect to track intensity minima in total internal reflection[115].

The subdiffraction size of dark spots underlies Nobel Prize-winning STED microscopy. A fluorescent particle is illuminated with a focused pump beam and a co-aligned depletion beam with a smaller, isolated dark spot. Fluorescence is suppressed wherever the depletion beam is bright. The effective point spread function is thus reduced to the dark region of the depletion beam, increasing spatial resolution while the focal spot is scanned[3,4]. Although STED microscopy does not strictly require a phase singularity – only a dark local minimum for the depletion beam – its contrast and efficiency improve when actual singularities are used. STED microscopy has achieved 3D spatial resolutions down to about $\lambda/10$. Further improvements have been limited by the localization precision of the fluorescent emission: for a Gaussian spot with a width of $\sigma(\lambda)$, which scales linearly with the emission wavelength, the localization precision of the Gaussian centroid is $\sigma(\lambda)/\sqrt{N}$, where N is the number of photons collected. High-resolution STED requires long integration times to increase N, during which the particle may photobleach or transition to other non-emitting states[116].

Balzarotti et al.[116] introduced MINFLUX, achieving an order-of-magnitude improvement in resolution[117,118] by localizing fluorescent molecules at a zero-intensity point rather than a maximum. With as few as four measurements at different positions of a scanning pump beam containing a phase singularity, MINFLUX estimates the particle position with precision scaling as $L/\sqrt{N}$, where L is a wavelength-independent length far smaller than $\sigma(\lambda)$ (ref. 116). Its low photon requirement enables rapid operation: it has resolved the walking dynamics of kinesin at 2-nm spatial and millisecond temporal resolution[119].

Micromanipulation

The intensity minima of phase singularities can trap and manipulate microparticles and cold atoms. Conventional single-beam traps use a tightly focused intensity maximum to hold high-index microparticles, whereas a doughnut (vortex) beam traps the particles that such a maximum cannot: absorptive and reflective particles, which can additionally be set rotating by OAM transfer[120] and glass spheres whose refractive index is lower than that of the surrounding medium[121]. Heckenberg et al.[122] and Yang et al.[123] review OAM-based micromechanical manipulation.

Phase singularities also trap cold atoms with blue-detuned light. Most cold atom traps use red-detuned light, which exerts an attractive force towards intensity maxima. Blue-detuned light is repulsive and traps atoms in intensity minima instead. Bazhenov et al.[124] first suggested that a low-intensity region could trap cold atoms, and such traps were soon realized using vortex modes[125,126].

Vectorial light fields with polarization singularities have also been examined for optical trapping. Cylindrical vector beams (CVBs) have polarization states with cylindrical symmetry around the optical axis. The two canonical CVBs are radially polarized and azimuthally polarized beams, both with a paraxial V-type singularity on axis. The radially polarized beam has an on-axis maximum of z-directed field at focus, whereas the azimuthally polarized beam has no E_z at focus, making its focal point also a non-paraxial V-type singularity. Tightly focused radially polarized traps outperform uniformly and azimuthally polarized traps in axial trapping efficiency because of reduced scattering forces[127,128]. This reduction lowers the laser power needed for stable trapping. CVBs have trapped beads in air[129], carbon nanotubes[130] and absorptive magnetic nanoparticles[131].

The tight localization of vortex-beam singularities has been used for micromachining ring-shaped structures with ultrashort pulses[132]. Hnatovsky et al.[133] showed that the longitudinal field component must be considered when ablating with tightly focused ultrashort pulses containing vortex modes. Duocastella and Arnold[134] review micromachining techniques with optical vortices.

Polarization fields also shape micromachining: ultrafast ablation with spatially varying polarization fields, such as vectorial vortex modes (radially and azimuthally polarized beams), can produce subwavelength grooves governed by the local linear polarization[135,136]. Such pulses can also structure transparent materials: Baltrukonis et al.[137] used a superposition of oppositely charged x-polarized and y-polarized vortices to fabricate 3D tubular structures with modified refractive indices, and Nacius et al.[138] reported that a C-type polarization singularity produces uniform flat-top beams with better performance in glass welding and thin-film removal than Gaussian beams.

Superoscillation profiling and control

Superoscillations are local wave behaviours in bandlimited functions that seem to contain Fourier components outside the function's frequency range. Singularities are closely connected to superoscillations: a superoscillation occurs near a singularity, and its properties are shaped by the singularity's geometry[34]. Optical singularities provide a means to control nearby superoscillations.

Glossary

Bandlimited function
A function whose Fourier transform vanishes outside a finite frequency interval.

Caustic
An envelope of a family of light rays, appearing as a bright line or surface of high ray density. Caustics are singularities of ray optics and are defined differently from the wave-optical singularities treated here.

Cross-spectral density
A complex-valued function describing the correlation between the fields at two points at a given frequency.

Diffeomorphism
A smooth, continuously invertible mapping that deforms one space into another without tearing.

Diffraction limit
The smallest feature an optical system can resolve, set by the wavelength and aperture (Rayleigh criterion is ~$1.22\lambda/D$ for an ideal circular aperture).

Jacobian determinant
The determinant of the matrix of first derivatives, here of the condition values with respect to the configuration coordinates. It measures local volume scaling and orientation.

Level set
The set of positions at which a field quantity takes one fixed value: a contour line (isoline) in two dimensions, a surface (isosurface) in three dimensions.

Möbius strip
A structure in which the major axis of the polarization ellipse twists through half a turn (or an odd number of half-turns) along a closed path around a polarization singularity.

Mutual coherence function
A complex-valued function describing the correlation between the fields at two points and two times.

Poincaré–Hopf index
A topological integer obtained by accumulating the polarization azimuth around a singularity on a closed surrounding path.

Point spread function
The intensity pattern an optical system produces from a point source; its shape and width are common measures of achievable resolution.

Skyrmion
A smooth, localized topological texture in which a field maps a region of physical or configuration space onto a space with a non-zero integer degree.

Skyrmionic hopfion
A three-dimensional topological texture in which every combination of polarization state and phase occurs exactly once within a confined volume. Singularity lines can organize the texture but do not define it.

Stokes parameters
Four measurable intensity combinations (S_0–S_3) that fully specify the paraxial polarization state of a monochromatic field.

Synthetic dimension
A controllable system parameter, such as wavelength or angle of incidence, treated as an additional coordinate of configuration space.

Weak measurement
A measurement based on weak coupling between a system and a measuring device, causing little disturbance but yielding little information in each trial.

Winding number
Number of times a closed curve in two-dimensional condition space encircles the origin, including its orientation.

Superoscillations have roots in antenna theory: Schelkunoff's subwavelength-spaced arrays[139] and Toraldo di Francia's super-gain pupil synthesis[140] produce far-field central lobes narrower than the open-aperture limit $\Delta\theta = 1.22\lambda/D$ by positioning far-field intensity zeros (Supplementary Fig. 2). The mathematical basis is the theory of superoscillation, which emerged later from the study of quantum weak measurements: Aharonov and collaborators[141] found anomalously large values arising from a bandlimited function oscillating faster than its highest Fourier components. Berry[142] studied such wave behaviour extensively and named it 'superoscillation'. Huang et al.[143] first linked superoscillations to subdiffraction focal spots, observing subwavelength hotspots in the near field of nanohole arrays.

Superoscillations require phase singularities. The large phase gradients $\nabla\phi$ around a phase singularity are themselves examples of superoscillations[144], which occur only near such singularities – consistent with their appearance in low-intensity regions of near-perfect destructive interference. The singularities are not always obvious: in the canonical superoscillatory function[145,146], $f(x) = (\cos x + ia\sin x)^N$, $a \in \mathbb{R}, N \in \mathbb{Z}$, defined on the real line, there are no apparent zeros. However, plotting the field in the complex plane reveals that the superoscillatory behaviour derives from nearby charge N singularities (Supplementary Information and Supplementary Fig. 3).

Although superoscillations have so far been connected only to phase singularities, a similar formalism may extend to higher-dimensional singular features associated with intensity minima, such as paraxial and non-paraxial V singularities.

Modelling phenomena

The topology of light around singularities can be mapped to other domains, making these fields convenient laboratory-scale proxies for more complex phenomena. For example, skyrmions, particle-like continuous fields in the 3D space, have analogous realizations in solid-state, high-energy and cosmological physics[22]. The large number of tunable parameters, such as frequency and beam tilt, can also serve as synthetic dimensions for modelling high-dimensional geometries[53,61]. Topologically nontrivial light can further excite topological collective states in atomic systems, which may be relevant to information transmission and quantum simulators[61,62].

Outlook

Optical singularities have already yielded powerful tools for imaging, microscopy and metrology, yet almost all of these exploit only the simplest phase singularities. The many empty cells in Supplementary Table 2, spanning combinations of configuration and condition dimension for which no singularity has yet been realized, show how much of the field remains open.

The clearest frontier lies in these higher-dimensional singularities. Because ordinary space offers only three Cartesian dimensions, singularities with a co-dimension above three become accessible only through synthetic dimensions such as wavelength or angle of incidence. Engineering stable singularities in these enlarged configuration spaces – together with the composite structures they support – would extend singular optics well beyond the phase vortex. Whether such structures hold up outside controlled conditions remains open: fundamental singularities persist in scattering media only while the perturbing field stays weaker than their stability strength, and their composites reorganize into other singularity types once the perturbation exceeds it.

Reaching that frontier will require the means to measure such fields. Realistic applications depend on the field surrounding a singularity as much as on the zero itself and so demand sensors with both high spatial resolution and tilt, or phase, sensitivity. Polarimetric wavefront sensors are a natural next step: they would enable full complex-field tomography of E_x, E_y, E_z, and with it, the tight localization of polarization singularities.

Published online: 21 September 2026

References

1. Berry, M. V. & Upstill, C. IV catastrophe optics: morphologies of caustics and their diffraction patterns. In *Progress in Optics XVIII* Vol. 18 (ed. Wolf, E.) 257–346 (Elsevier, 1980).
2. Nye, J. F. *Natural Focusing and Fine Structure of Light* (Institute of Physics Publishing, 1999).
3. Hell, S. W. & Wichmann, J. Breaking the diffraction resolution limit by stimulated emission: stimulated-emission-depletion fluorescence microscopy. *Opt. Lett.* **19**, 780–782 (1994).
4. Willig, K. I., Harke, B., Medda, R. & Hell, S. W. STED microscopy with continuous wave beams. *Nat. Methods* **4**, 915–918 (2007).
5. Nye, J. F. & Berry, M. Dislocations in Wave Trains. *Proc. R. Soc. A* **336**, 165–190 (1974).
This is the founding paper of singular optics, showing that interfering waves inevitably contain lines where the amplitude vanishes and the phase is undefined, and classifying their local geometry by analogy with edge and screw dislocations in crystals.
6. Hajnal, J. V. Singularities in the transverse fields of electromagnetic waves. I. Theory. *Proc. R. Soc. A* **414**, 433–446 (1987).
7. Hajnal, J. V. Singularities in the transverse fields of electromagnetic waves. II. Observations on the electric field. *Proc. R. Soc. A* **414**, 447–468 (1987).
8. Freund, I. Polarization singularity indices in Gaussian laser beams. *Opt. Commun.* **201**, 251–270 (2002).
9. Berry, M. V. Circular lines of circular polarization in three dimensions, and their transverse-field counterparts. *J. Opt.* **15**, 044024 (2013).
10. Nye, J. F. & Hajnal, J. V. The wave structure of monochromatic electromagnetic radiation. *Proc. R. Soc. A* **409**, 21–36 (1987).
This paper extends optical singularities from scalar waves into full three-dimensional vector fields, identifying which polarization features are structurally stable: lines of circular polarization, lines of linear polarization, and surfaces separating regions of opposite handedness.
11. Chen, W., Chen, Y. & Liu, W. Line singularities and Hopf indices of electromagnetic multipoles. *Laser Photon. Rev.* **14**, 2000049 (2020).
12. Shvedov, V. & Krolikowski, W. Instantaneous field singularities in electromagnetic waves. *New J. Phys.* **20**, 103034 (2018).
13. Nye, J. F. Lines of circular polarization in electromagnetic wave fields. *Proc. R. Soc. A* **389**, 279–290 (1983).
14. Freund, I. Polarization flowers. *Opt. Commun.* **199**, 47–63 (2001).
15. Basistiy, I. V., Pas'ko, V. A., Slyusar, V. V., Soskin, M. S. & Vasnetsov, M. V. Synthesis and analysis of optical vortices with fractional topological charges. *J. Opt. A* **6**, S166–S169 (2004).
16. Berry, M. V. Optical vortices evolving from helicoidal integer and fractional phase steps. *J. Opt. A* **6**, 259–268 (2004).
17. Leach, J., Yao, E. & Padgett, M. J. Observation of the vortex structure of a non-integer vortex beam. *New J. Phys.* **6**, 71 (2004).
18. Ostrovsky, A. S., Rickenstorff-Parrao, C. & Arrizón, V. Generation of the 'perfect' optical vortex using a liquid-crystal spatial light modulator. *Opt. Lett.* **38**, 534–536 (2013).
19. Berry, M. V. & Dennis, M. R. Knotted and linked phase singularities in monochromatic waves. *Proc. R. Soc. A* **457**, 2251–2263 (2001).
20. Bauer, T. et al. Observation of optical polarization Möbius strips. *Science* **347**, 964–966 (2015).
21. Tekce, K., Otte, E. & Denz, C. Optical singularities and Möbius strip arrays in tailored non-paraxial light fields. *Opt. Express* **27**, 29685–29696 (2019).
22. Sugic, D. et al. Particle-like topologies in light. *Nat. Commun.* **12**, 6785 (2021).
23. Shen, Y., Hou, Y., Papasimakis, N. & Zheludev, N. I. Supertoroidal light pulses as electromagnetic skyrmions propagating in free space. *Nat. Commun.* **12**, 5891 (2021).
24. Wang, H., Wojcik, C. C. & Fan, S. Topological spin defects of light. *Optica* **9**, 1417–1423 (2022).
This paper introduces a singularity with a rare co-dimension of three: a point where all three components of the spin density vanish, surrounded by a spin pattern that winds around it and so carries a quantized charge.
25. Smith, D. R., Padilla, W. J., Vier, D. C., Nemat-Nasser, S. C. & Schultz, S. Composite medium with simultaneously negative permeability and permittivity. *Phys. Rev. Lett.* **84**, 4184–4187 (2000).
26. Bomzon, Z., Kleiner, V. & Hasman, E. Pancharatnam–Berry phase in space-variant polarization-state manipulations with subwavelength gratings. *Opt. Lett.* **26**, 1424–1426 (2001).
27. Yu, N. & Capasso, F. Flat optics with designer metasurfaces. *Nat. Mater.* **13**, 139–150 (2014).
28. Dorrah, A. H. & Capasso, F. Tunable structured light with flat optics. *Science* **376**, eabi6860 (2022).
29. Zhang, Y., Yang, X. & Gao, J. Generation of polarization singularities with geometric metasurfaces. *Sci. Rep.* **9**, 19656 (2019).
30. Ren, H. et al. Metasurface orbital angular momentum holography. *Nat. Commun.* **10**, 2986 (2019).
31. Lim, S. W. D., Park, J.-S., Meretska, M. L., Dorrah, A. H. & Capasso, F. Engineering phase and polarization singularity sheets. *Nat. Commun.* **12**, 4190 (2021).
This paper shows how singularities can be sculpted into unstable, sheet-like geometries by maximizing how steeply the phase varies, and realizes sheets with heart-shaped cross-sections using metasurfaces.
32. Lim, S. W. D. et al. Point singularity array with metasurfaces. *Nat. Commun.* **14**, 3237 (2023).
33. Spaegele, C. M. et al. Topologically protected optical polarization singularities in four-dimensional space. *Sci. Adv.* **9**, eadh0369 (2023).
This paper realizes a singularity that needs four conditions to vanish (co-dimension four), which cannot be stable in ordinary three-dimensional space but becomes stable once wavelength is added as a fourth dimension, making synthetic dimensions a practical design resource.
34. Gbur, G. J. *Singular Optics* (CRC Press, 2016).
35. Simon, D. S. *Topology in Optics* (IOP Publishing, 2021).
36. Soskin, M. S. & Vasnetsov, M. V. Singular optics. In *Progress in Optics* Vol. 42 (ed. Wolf, E.) 219–276 (Elsevier BV, 2001).
37. Dennis, M. R. *Topological Singularities in Wave Fields*. PhD thesis, Univ. Bristol (2001).
This thesis gives a comprehensive account of how wave singularities are classified in scalar, vector and tensor fields, organized by how many conditions must vanish at a point and whether the result survives perturbation.
38. Dennis, M. R., O'Holleran, K. & Padgett, M. J. Singular optics: optical vortices and polarization singularities. In *Progress in Optics* Vol. 53 (ed. Wolf, E.) 293–363 (Elsevier BV, 2009).
39. Shen, Y. et al. Optical vortices 30 years on: OAM manipulation from topological charge to multiple singularities. *Light. Sci. Appl.* **8**, 90 (2019).
40. Otte, E. & Denz, C. Customization and analysis of structured singular light fields. *J. Opt.* **23**, 073501 (2021).
41. Courtial, J., Dholakia, K., Allen, L. & Padgett, M. J. Gaussian beams with very high orbital angular momentum. *Opt. Commun.* **144**, 210–213 (1997).
42. Berry, M. V. & Liu, W. No general relation between phase vortices and orbital angular momentum. *J. Phys. A Math. Theor.* **55**, 374001 (2022).
43. Berry, M. V. Waves and Thom's theorem. *Adv. Phys.* **25**, 1–26 (1976).
44. Dennis, M. R. Rows of optical vortices from elliptically perturbing a high-order beam. *Opt. Lett.* **31**, 1325 (2006).
45. Arlt, J. & Padgett, M. J. Generation of a beam with a dark focus surrounded by regions of higher intensity: the optical bottle beam. *Opt. Lett.* **25**, 191–193 (2000).
46. Ni, J. et al. Multidimensional phase singularities in nanophotonics. *Sci.* **374**, eabj0039 (2021).
47. Devlin, R. C., Ambrosio, A., Rubin, N. A., Mueller, J. P. B. & Capasso, F. Arbitrary spin-to-orbital angular momentum conversion of light. *Science* **358**, 896–901 (2017).
48. Maguid, E. et al. Photonic spin-controlled multifunctional shared-aperture antenna array. *Science* **352**, 1202–1206 (2016).
49. Liu, W., Liu, W., Shi, L. & Kivshar, Y. Topological polarization singularities in metaphotonics. *Nanophotonics* **10**, 1469–1486 (2021).
50. Intaravanne, Y. et al. Color-selective three-dimensional polarization structures. *Light. Sci. Appl.* **11**, 302 (2022).
51. Desyatnikov, A. S., Kivshar, Y. S. & Torner, L. Optical vortices and vortex solitons. In *Progress in Optics* Vol. 47 (ed. Wolf, E.) 291–391 (Elsevier, 2005).
52. Kivshar, Y. Dark optical solitons: physics and applications. *Phys. Rep.* **298**, 81–197 (1998).
53. Yuan, L., Lin, Q., Xiao, M. & Fan, S. Synthetic dimension in photonics. *Optica* **5**, 1396–1405 (2018).
54. Bliokh, K. Y. & Nori, F. Spatiotemporal vortex beams and angular momentum. *Phys. Rev. A* **86**, 033824 (2012).
55. Berry, M. V. & Shukla, P. Geometry of 3D monochromatic light: local wavevectors, phases, curl forces, and superoscillations. *J. Opt.* **21**, 064002 (2019).
56. Otte, E., Alpmann, C. & Denz, C. Polarization singularity explosions in tailored light fields. *Laser Photon. Rev.* **12**, 1700200 (2018).
57. Schouten, H. F., Gbur, G., Visser, T. D. & Wolf, E. Phase singularities of the coherence functions in Young's interference pattern. *Opt. Lett.* **28**, 968–970 (2003).
58. Maleev, I. D., Palacios, D. M., Marathay, A. S. & Swartzlander, G. A. Jr. Spatial correlation vortices in partially coherent light: theory. *J. Optical Soc. Am. B* **21**, 1895–1900 (2004).
59. Dennis, M. R., King, R. P., Jack, B., O'Holleran, K. & Padgett, M. J. Isolated optical vortex knots. *Nat. Phys.* **6**, 118–121 (2010).
60. Larocque, H. et al. Reconstructing the topology of optical polarization knots. *Nat. Phys.* **14**, 1079–1082 (2018).
61. Ehrmanntraut, D. et al. Optical second-order skyrmionic hopfion. *Optica* **10**, 725–731 (2023).
62. Parmee, C. D., Dennis, M. R. & Ruostekoski, J. Optical excitations of Skyrmions, knotted solitons, and defects in atoms. *Commun. Phys.* **5**, 54 (2022).
63. Shen, Y. et al. Optical skyrmions and other topological quasiparticles of light. *Nat. Photonics* **18**, 15–25 (2024).

64. Basistiy, I. V., Bazhenov, V. Y., Soskin, M. S. & Vasnetsov, M. V. Optics of light beams with screw dislocations. *Opt. Commun.* **103**, 422–428 (1993).
65. Dehghan, N., D'Errico, A., Jaouni, T. & Karimi, E. Effects of aberrations on 3D optical topologies. *Commun. Phys.* **6**, 357 (2023).
66. Pires, D. G. et al. Stability of optical knots in atmospheric turbulence. *Nat. Commun.* **16**, 3001 (2025).
67. Schwarz, A. *Topology for Physicists*. *Media* (Springer-Verlag, 1994).
68. Berry, M. V. Index formulae for singular lines of polarization. *J. Opt. A* **6**, 675–678 (2004).
69. Berry, M. V. & Dennis, M. R. Phase singularities in isotropic random waves. *Proc. R. Soc. A* **456**, 2059–2079 (2000).
70. Berry, M. V. & Dennis, M. R. Knotting and unknotting of phase singularities: Helmholtz waves, paraxial waves and waves in 2+1 spacetime. *J. Phys. A Math. Gen.* **34**, 8877–8888 (2001).
71. Allen, L., Beijersbergen, M. W., Spreeuw, R. J. C. & Woerdman, J. P. Orbital angular momentum of light and the transformation of Laguerre–Gaussian laser modes. *Phys. Rev. A* . **45**, 8185–8189 (1992).
72. Wang, H., Guo, C., Jin, W., Song, A. Y. & Fan, S. Engineering arbitrarily oriented spatiotemporal optical vortices using transmission nodal lines. *Optica* **8**, 966–971 (2021).
73. Dorrah, A. H., Zamboni-Rached, M. & Mojahedi, M. Controlling the topological charge of twisted light beams with propagation. *Phys. Rev. A* **93**, 063864 (2016).
74. Otte, E., Alpmann, C. & Denz, C. Higher-order polarization singularities in tailored vector beams. *J. Opt.* **18**, 074012 (2016).
75. Dorrah, A. H., Rubin, N. A., Tamagnone, M., Zaidi, A. & Capasso, F. Structuring total angular momentum of light along the propagation direction with polarization-controlled meta-optics. *Nat. Commun.* **12**, 6249 (2021).
76. Aborahama, Y., Dorrah, A. H. & Mojahedi, M. Designing the phase and amplitude of scalar optical fields in three dimensions. *Opt. Express* **28**, 24721–24730 (2020).
77. Maurer, C., Jesacher, A., Fürhapter, S., Bernet, S. & Ritsch-Marte, M. Tailoring of arbitrary optical vector beams. *New J. Phys.* **9**, 78–78 (2007).
78. Hajnal, J. V. Observations of singularities in the electric and magnetic fields of freely propagating microwaves. *Proc. R. Soc. A* **430**, 413–421 (1990).
79. Kumar, V., Philip, G. M. & Viswanathan, N. K. Formation and morphological transformation of polarization singularities: hunting the monstar. *J. Opt.* **15**, 044027 (2013).
80. Marrucci, L., Manzo, C. & Paparo, D. Optical spin-to-orbital angular momentum conversion in inhomogeneous anisotropic media. *Phys. Rev. Lett.* **96**, 163905 (2006).
81. Heckenberg, N. R., McDuff, R., Smith, C. P. & White, A. G. Generation of optical phase singularities by computer-generated holograms. *Opt. Lett.* **17**, 221–223 (1992).
82. Schoonover, R. W. & Visser, T. D. Creating polarization singularities with an N-pinhole interferometer. *Phys. Rev. A* **79**, 043809 (2009).
83. Ruchi Pal, S. K. & Senthilkumaran, P. Generation of V-point polarization singularity lattices. *Opt. Express* **25**, 19326–19331 (2017).
84. Wang, B. et al. Generating optical vortex beams by momentum-space polarization vortices centred at bound states in the continuum. *Nat. Photonics* **14**, 623–628 (2020).
85. Alpmann, C., Schlickriede, C., Otte, E. & Denz, C. Dynamic modulation of Poincaré beams. *Sci. Rep.* **7**, 8076 (2017).
86. Kurzynowski, P., Woźniak, W. A. & Borwińska, M. Regular lattices of polarization singularities: their generation and properties. *J. Opt.* **12**, 035406 (2010).
87. Beckley, A. M., Brown, T. G. & Alonso, M. A. Full Poincaré beams. *Opt. Express* **18**, 10777–10785 (2010).
88. Shaltout, A. M., Shalaev, V. M. & Brongersma, M. L. Spatiotemporal light control with active metasurfaces. *Science* **364**, eaat3100 (2019).
89. Campbell, S. D. et al. Review of numerical optimization techniques for meta-device design [invited]. *Opt. Mater. Express* **9**, 1842–1863 (2019).
90. Li, Z., Pestourie, R., Lin, Z., Johnson, S. G. & Capasso, F. Empowering metasurfaces with inverse design: principles and applications. *ACS Photonics* **9**, 2178–2192 (2022).
91. Foo, G., Palacios, D. M. & Swartzlander, G. A. Optical vortex coronagraph. *Opt. Lett.* **30**, 3308 (2005).
This paper proposes a coronagraph in which a phase singularity placed at a telescope focus removes the light of an on-axis star across the whole exit pupil, while light from a dim off-axis companion passes through.
92. Gibson, G. et al. Free-space information transfer using light beams carrying orbital angular momentum. *Opt. Express* **12**, 5448–5456 (2004).
93. Wang, J. Advances in communications using optical vortices. *Photonics Res.* **4**, B14–B28 (2016).
94. Wang, J. et al. Terabit free-space data transmission employing orbital angular momentum multiplexing. *Nat. Photonics* **6**, 488–496 (2012).
95. Bozinovic, N. et al. Terabit-scale orbital angular momentum mode division multiplexing in fibers. *Science* **340**, 1545–1548 (2013).
96. Ndagano, B., Nape, I., Cox, M. A., Rosales-Guzman, C. & Forbes, A. Creation and detection of vector vortex modes for classical and quantum communication. *J. Lightwave Technol.* **36**, 292–301 (2018).
97. Vallone, G. et al. Free-space quantum key distribution by rotation-invariant twisted photons. *Phys. Rev. Lett.* **113**, 060503 (2014).
98. Mirhosseini, M. et al. High-dimensional quantum cryptography with twisted light. *New J. Phys.* **17**, 033033 (2015).
99. Ndagano, B. et al. A deterministic detector for vector vortex states. *Sci. Rep.* **7**, 13882 (2017).
100. Bouchard, F. et al. Quantum cryptography with twisted photons through an outdoor underwater channel. *Opt. Express* **26**, 22563 (2018).
101. Cozzolino, D. et al. Orbital angular momentum states enabling fiber-based high-dimensional quantum communication. *Phys. Rev. Appl.* **11**, 064058 (2019).
102. Bechmann-Pasquinucci, H. & Tittel, W. Quantum cryptography using larger alphabets. *Phys. Rev. A* . **61**, 062308 (2000).
103. Cerf, N. J., Bourennane, M., Karlsson, A. & Gisin, N. Security of quantum key distribution using d-level systems. *Phys. Rev. Lett.* **88**, 127902 (2002).
104. Otte, E., White, A. D., Güsken, N. A., Vučković, J. & Brongersma, M. L. Tunable vector beam decoder by inverse design for high-dimensional quantum key distribution with 3D polarized spatial modes. Preprint at https://doi.org/10.48550/arXiv.2304.12296 (2023).
105. Zuravlev, V. A., Kobozev, I. K. & Kravtsov, Y. A. Statistical characteristics of phase front dislocations of a wave field. *Zh. Eksp. Teor. Fiz.* **102**, 483–495 (1992).
106. Aksenov, V., Banakh, V. & Tikhomirova, O. Potential and vortex features of optical speckle fields and visualization of wave-front singularities. *Appl. Opt.* **37**, 4536–4540 (1998).
107. Wackerman, C. C. & Yagle, A. E. Phase retrieval and estimation with use of real-plane zeros. *J. Optical Soc. Am. A* **11**, 2016–2026 (1994).
108. Chen, P.-T. & Fiddy, M. A. Image reconstruction from power spectral data with use of point-zero locations. *J. Optical Soc. Am. A* **11**, 2210–2214 (1994).
109. Swartzlander, G. A. Peering into darkness with a vortex spatial filter. *Opt. Lett.* **26**, 497–499 (2001).
110. Mawet, D., Riaud, P., Absil, O. & Surdej, J. Annular groove phase mask coronagraph. *Astrophys. J.* **633**, 1191–1200 (2005).
111. Serabyn, E. et al. The W. M. Keck Observatory infrared vortex coronagraph and a first image of HIP 79124 B. *Astron. J.* **153**, 43 (2017).
112. Yuan, G. H. & Zheludev, N. I. Detecting nanometric displacements with optical ruler metrology. *Science* **364**, 771–775 (2019).
113. Liu, T. et al. Picophotonic localization metrology beyond thermal fluctuations. *Nat. Mater.* **22**, 844–847 (2023).
114. Xiao, J. & Ha, T. Flipping nanoscopy on its head. *Science* **355**, 582–584 (2017).
115. Wolter, H. Zur Frage des Lichtweges bei Totalreflexion. *Z. für Naturforschung A* **5**, 276–283 (1950).
116. Balzarotti, F. et al. Nanometer resolution imaging and tracking of fluorescent molecules with minimal photon fluxes. *Science* **355**, 606–612 (2017).
This paper demonstrates how a zero locates an object better than a peak: MINFLUX finds a single fluorescent molecule by scanning the dark centre of a doughnut beam across it rather than fitting the centre of a bright spot, using 22 times fewer photons and achieving higher spatial resolution.
117. Schmidt, R. et al. MINFLUX nanometer-scale 3D imaging and microsecond-range tracking on a common fluorescence microscope. *Nat. Commun.* **12**, 1478 (2021).
118. Eilers, Y., Ta, H., Gwosch, K. C., Balzarotti, F. & Hell, S. W. MINFLUX monitors rapid molecular jumps with superior spatiotemporal resolution. *Proc. Natl Acad. Sci.* **115**, 6117–6122 (2018).
119. Deguchi, T. et al. Direct observation of motor protein stepping in living cells using MINFLUX. *Science* **379**, 1010–1015 (2023).
120. He, H., Heckenberg, N. R. & Rubinsztein-Dunlop, H. Optical particle trapping with higher-order doughnut beams produced using high efficiency computer generated holograms. *J. Mod. Opt.* **42**, 217–223 (1995).
121. Gahagan, K. T. & Swartzlander, G. A. Optical vortex trapping of particles. *Opt. Lett.* **21**, 827–829 (1996).
122. Heckenberg, N. R., Friese, M. E. J., Nieminen, T. A. & Rubinsztein-Dunlop, H. Mechanical effects of optical vortices. In *Optical Vortices* (eds Vasnetsov, M. & Staliunas, K.) 75–105 (Nova Science, 1999).
123. Yang, Y., Ren, Y.-X., Chen, M., Arita, Y. & Rosales-Guzmán, C. Optical trapping with structured light: a review. *Adv. Photonics* **3**, 034001 (2021).
124. Bazhenov, V. Y. U., Soskin, M. S. & Vasnetsov, M. V. Screw dislocations in light wavefronts. *J. Mod. Opt.* **39**, 985–990 (1992).
125. Kuga, T. et al. Novel optical trap of atoms with a doughnut beam. *Phys. Rev. Lett.* **78**, 4713–4716 (1997).
This paper demonstrates a singularity used as a container: laser-cooled rubidium atoms are held in the dark core of a doughnut beam tuned so that the light repels them.
126. Yin, J., Zhu, Y., Wang, W., Wang, Y. & Jhe, W. Optical potential for atom guidance in a dark hollow laser beam. *J. Optical Soc. Am. B* **15**, 25–33 (1998).
127. Nieminen, T. A., Heckenberg, N. R. & Rubinsztein-Dunlop, H. Forces in optical tweezers with radially and azimuthally polarized trapping beams. *Opt. Lett.* **33**, 122 (2008).
128. Kawauchi, H., Yonezawa, K., Kozawa, Y. & Sato, S. Calculation of optical trapping forces on a dielectric sphere in the ray optics regime produced by a radially polarized laser beam. *Opt. Lett.* **32**, 1839 (2007).
129. Michihata, M., Hayashi, T. & Takaya, Y. Measurement of axial and transverse trapping stiffness of optical tweezers in air using a radially polarized beam. *Appl. Opt.* **48**, 6143 (2009).
130. Donato, M. G. et al. Optical trapping of nanotubes with cylindrical vector beams. *Opt. Lett.* **37**, 3381 (2012).
131. Zhong, M.-C. et al. Optical trapping of core-shell magnetic microparticles by cylindrical vector beams. *Appl. Phys. Lett.* **105**, 181112 (2014).
132. Hamazaki, J. et al. Optical-vortex laser ablation. *Opt. Express* **18**, 2144–2151 (2010).
133. Hnatovsky, C., Shvedov, V. G., Shostka, N., Rode, A. V. & Krolikowski, W. Polarization-dependent ablation of silicon using tightly focused femtosecond laser vortex pulses. *Opt. Lett.* **37**, 226–228 (2012).

134. Duocastella, M. & Arnold, C. B. Bessel and annular beams for materials processing. *Laser Photon. Rev.* **6**, 607–621 (2012).
135. Lou, K. et al. Two-dimensional microstructures induced by femtosecond vector light fields on silicon. *Opt. Express* **20**, 120 (2012).
136. Anoop, K. K. et al. Femtosecond laser surface structuring of silicon using optical vortex beams generated by a *q*-plate. *Appl. Phys. Lett.* **104**, 241604 (2014).
137. Baltrukonis, J., Ulčinas, O., Orlov, S. & Jukna, V. High-order vector Bessel-Gauss beams for laser micromachining of transparent materials. *Phys. Rev. Appl.* **16**, 034001 (2021).
138. Nacius, E., Ulčinas, O., Orlov, S. & Jukna, V. Polarization singularities for shaping of vector flat-top beams in utilization for high-power laser micromachining of various materials. *Opt. Laser Technol.* **177**, 111133 (2024).
139. Schelkunoff, S. A. A mathematical theory of linear arrays. *Bell Syst. Technical J.* **22**, 80–107 (1943).
140. Toraldo di Francia, G. Super-gain antennas and optical resolving power. *Il Nuovo Cimento* **9**, 426–438 (1952).
This paper is the origin of the idea that zeros can be placed on purpose: dividing a lens pupil into concentric rings of chosen transmission forces the intensity to vanish at selected angles and narrows the central focal spot below the diffraction limit, decades before superoscillation was named.
141. Aharonov, Y., Albert, D. Z. & Vaidman, L. How the result of a measurement of a component of the spin of a spin-1/2 particle can turn out to be 100. *Phys. Rev. Lett.* **60**, 1351–1354 (1988).
142. Berry, M. Faster than Fourier. In *Quantum Coherence and Reality* (eds Anandan J. S. & Safko, J. L.) 55–65 (World Scientific, 1995).
143. Huang, F. M., Chen, Y., Garcia de Abajo, F. J. & Zheludev, N. I. Optical super-resolution through super-oscillations. *J. Opt. A* **9**, S285–S288 (2007).
144. Berry, M. V. & Dennis, M. R. Natural superoscillations in monochromatic waves in *D* dimensions. *J. Phys. A Math. Theor.* **42**, 022003 (2009).
145. Berry, M. V. & Popescu, S. Evolution of quantum superoscillations and optical superresolution without evanescent waves. *J. Phys. A Math. Gen.* **39**, 6965–6977 (2006).
146. Berry, M. et al. Roadmap on superoscillations. *J. Opt.* **21**, 053002 (2019).

Acknowledgements
The authors thank A. H. Dorrah for feedback. This material is based on work supported by the Air Force Office of Scientific Research under award numbers FA9550-21-1-0312 (to F.C.) and FA9550-22-1-0243 (to F.C.). S.W.D.L. is supported by the Schmidt Science Fellows, in partnership with the Rhodes Trust. S.W.D.L. is also supported by A*STAR Singapore through the National Science Scholarship Scheme.

Author contributions
All authors contributed to the writing, critical review and editing of this manuscript. All authors have read and approved the final version.

Competing interests
The authors declare no competing interests.

Additional information
Supplementary information The online version contains supplementary material available at https://doi.org/10.1038/s44287-026-00331-5.

Peer review information *Nature Reviews Electrical Engineering* thanks the anonymous reviewer(s) for their contribution to the peer review of this work.